A NUMERICAL SIMULATION OF BLOOD FLOW DYNAMICS IN CORONARY ARTERY USING STREAMFUNCTION-VORTICITY FORMULATION

Leandro Marques, marquesleandro67@gmail.com[1]
Gustavo Anjos, gustavo.anjos@uerj.br[1]
José Pontes, jose.pontes@uerj.br[1]

[1]State University of Rio de Janeiro - UERJ, R. Fonseca Teles 524, 20550-013, Rio de Janeiro, Brazil

Abstract: The present work aims at developing a computational framework to simulate coronary artery flows in cartesian coordinates. An accurate method capable of capturing the flow dynamics is strictly required. In this paper a Finite Element Method (FEM) is used to solve the governing equations of the motion of the blood flow found in coronary artery as incompressible fluid using the stream-vorticity formulation with coupled mass transport.
Keywords: Finite Element Method, Taylor-Galerkin Method, Biomedical Engineering, Hemodynamics, Atherosclerosis.

1. INTRODUCTION

According to the World Health Organization (2017), more people die annually from the cardiovascular diseases (CVDs) that from any other cause in the world. An estimated 17.7 million people died from CVDs in 2015, representing 31% of all global deaths. About 41% of these deaths were due to coronary artery disease (CAD). The leading cause of the CAD is atherosclerosis where the diameter of the vessel is decreased. Two treatments can be performed: coronary artery bypass grafting (CABG) or percutaneous transluminal coronary angioplasty (PTCA). The PTCA is a minimally invasive procedure where a small wire tube, called stents, is placed. This work aims to know how the dynamics of blood flow in coronary artery with atherosclerosis and with stents struts placed.

The dynamics of blood flow in coronary artery and possible influence of stents struts with computational fluid dynamics (CFD) requires a robust numerical method to compute the solution of the differential equations in a relevant model. We consider the model of dissolution and transport of sirolimus on a two-dimensional domain representing the polymer coating layer and the hydrodynamic of the blood flow in the artery in the vicinity of a stent strut as suggested by Bozsak *et al.* (2014) and McGinty and Pontrelli (2016). Also, the effect of the releasing process of the polymers is considered. However, the spatial distribution of the sirolimus is greatly influenced by the flow and the arterial wall properties, being therefore susceptible to patient health conditions. The difference of artery shapes and existence of the struts have been investigated in 4 test cases in the influence on the flow dynamics and the transport of a chemical species as suggested by Wang *et al.* (2017).

We employ the Finite Element method on an unstructured mesh created by open source software called *GMSH* proposed by Geuzaine and Remacle (2009) for the discretization of the incompressible single-phase Navier-Stokes through the stream-vorticity function coupled with the concentration equation. We apply the Taylor-Galerkin method to the decrease the spurious oscillations as seen for moderate to high Reynolds numbers as proposed by Donea (1984) and Zienkiewicz and Taylor (2000) and was used the well-known benchmark problem lid-driven cavity for the validation of the numerical code where the results were compared with Ghia *et al.* (1982) and Marchi *et al.* (2009).

2. MATHEMATICAL MODEL

A 2-dimensional Finite Element Method approach is employed to analyse the dynamics of blood flow in coronary artery and possible influence of stents struts. The first step in its development is the initial modelling of the problem, and in this case it can be described by a formulation using the vorticity and stream function applied in the conservation of momentum equation for incompressible flow and the concentration distribution equation. This approach makes the model useful for the cases of single-phase flows.

$$\frac{\partial w}{\partial t} + \mathbf{v}.\nabla w = \frac{1}{Re}\nabla^2 w \qquad (1)$$

$$\nabla^2 \psi = -w \tag{2}$$

$$\mathbf{v} = \mathbf{D}\psi \tag{3}$$

$$\frac{\partial c}{\partial t} + \mathbf{v}.\nabla c = \frac{1}{ReSc}\nabla^2 c \tag{4}$$

Where, ω is the vorticity field, ψ is the stream function field, c is the concentration field, $\mathbf{v} = (u, v)$ is the velocity field, $\mathbf{D} = [\partial/\partial y, -\partial/\partial x]$ is a mathematical operator, $Re = \rho u D/\mu$ is the Reynolds number, $Sc = \nu/D$ is the Schmidt number, x and y are the independent spatial variables and t is the time variable.

2.1 Initial and Boundary Conditions

As commented by Anjos (2012), the initial conditions and the boundary conditions are of utmost importance to realistically characterizing any problem modeled by differential equations. Thus, the boundary conditions used in this paper are briefly explained below:

- *inflow condition*: the normal velocity component is set to null value $v = 0$. The derivates of the streamfunction and the concentration are set null values $\partial\psi/\partial n = 0$ and $\partial c/\partial n = 0$ respectively. For the tangent velocity component is set a half parabolic profile comes from the analytical solution of a Straight Channel in the cartesian coordinates: $u = u_{max}(1 - (y/R)^2)$, where $u_{max} = 2$.

- *No-slip condition*: all the velocity componentes are specified with null value $u = 0$ and $v = 0$. The streamfunction is also specified $\psi = 1.3$. The derivative concentration is set null value $\partial c/\partial n = 0$.

- *outflow condition*: no value is specified. The derivatives of the tangent velocity component, of the normal velocity component, of streamfunction and of concentration are set to null values, that is, $\partial u/\partial n = 0$, $\partial v/\partial n = 0$, $\partial\psi/\partial n = 0$ and $\partial c/\partial n = 0$ respectively.

- *Free-slip condition*: used when a symmetry condition is desired. The normal velocity component is set to null value $v = 0$ as well as the streamfunction $\psi = 0$. The derivative of the tangent velocity component and the derivative of the concentration are also set to null value $\partial u/\partial n = 0$ and $\partial c/\partial n = 0$ respectively.

- *Strut condition*: used on the stent. The normal velocity component and the tangent velocity component are specified with null value $u = 0$ and $v = 0$. The streamfunction and the concentration are also specified $\psi = 1.3$ and $c = 1$ respectively.

The boundary condition of the vorticity field is calculated in the solution algorithm scheme as we will see later.

2.2 Finite Element Method

This is paper, was used the Galerkin formulation to discretize the government equations. The spatial domain was discretized using linear triangular elements by open source software called GMSH proposed by Geuzaine and Remacle (2009). For the discretization of the temporal domain was used a finite differences method with a forward difference approximation and the Taylor-Galerkin Method with omitted terms of higher order than two was used to the decrease the spurious oscillations for moderate to high Reynolds numbers as proposed by Donea (1984) and Zienkiewicz and Taylor (2000). Therefore, the governing equations in matrix form used in this paper were:

$$\begin{aligned}
\left[\frac{M}{\Delta t} + \frac{1}{Re}\left[K_{xx} + K_{yy}\right]\right]w^{n+1} &= \frac{M}{\Delta t}w^n - u \cdot G_x w^n - v \cdot G_y w^n \\
&- u\frac{\Delta t}{2}\left[uK_{xx} + vK_{xy}\right]w^n - v\frac{\Delta t}{2}\left[uK_{yx} + vK_{yy}\right]w^n
\end{aligned} \tag{5}$$

$$\left[K_{xx} + K_{yy}\right]\psi = Mw \tag{6}$$
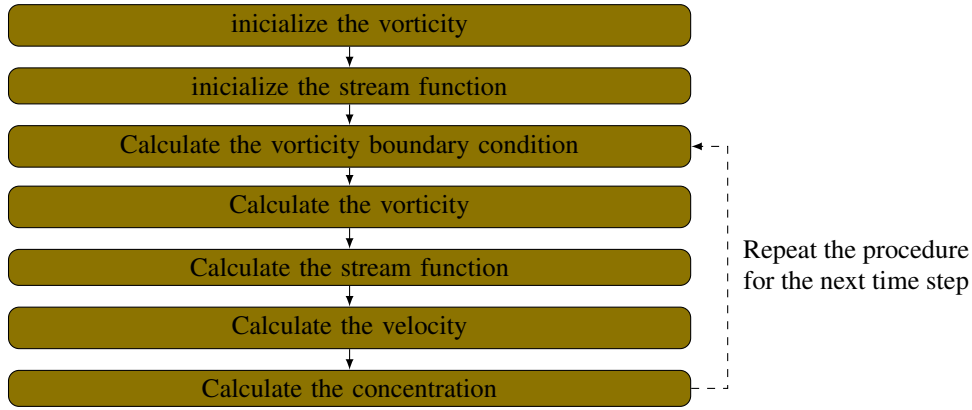
$$Mu = G_y\psi \tag{7}$$

$$Mv = -G_x\psi \tag{8}$$

$$\left[\frac{M}{\Delta t} + \frac{1}{ReSc}\left[K_{xx} + K_{yy}\right]\right]c^{n+1} = \frac{M}{\Delta t}c^n - u \cdot G_x c^n - v \cdot G_y c^n$$
$$- u\frac{\Delta t}{2}\left[uK_{xx} + vK_{xy}\right]c^n - v\frac{\Delta t}{2}\left[uK_{yx} + vK_{yy}\right]c^n \tag{9}$$

Where, M is mass matrix, G_x and G_y are gradient matrix, K_{xx}, K_{xy}, K_{yx} and K_{yy} are stiffness matrix. The last term of the Eqs. 5 and 9 is known as numerical diffusion and it decrease the spurious oscillations as seen for moderate to high Reynolds numbers. For scalars, *Taylor Galerkin Method* and *Characteristic Galerkin* produce the same result as showed by Lohner *et al.* (1984). The superscripts *n+1* and *n* are the scalar that will be calculated and that was calculated in the previous time step, respectively.

2.3 Numerical Solution

The linear system of equations that come from implementing the FEM is solved throught iterative method *Conjugate Gradient Solver* available in the public library for scientific tools *SciPy* maintained by Jones *et al.* (2001) in the Python language. The solution algorithm used is shown below:

inicialize the vorticity

inicialize the stream function

Calculate the vorticity boundary condition

Calculate the vorticity

Calculate the stream function

Calculate the velocity

Calculate the concentration

Repeat the procedure for the next time step

that is:

1. **Inicialize the vorticity with the equation:**

$$Mw = G_x v - G_y u$$

2. **Inicialize the stream function with the equation:**

$$\left[K_{xx} + K_{yy}\right]\psi = Mw$$

   It is necessary to apply the boundary condition in the equation.

3. **Calculate the vorticity boundary condition with the equation:**

$$Mw = G_x v - G_y u$$

4. **Calculate the vorticity with the equation:**

$$\left[\frac{M}{\Delta t} + \frac{1}{Re}\left[K_{xx} + K_{yy}\right]\right]w^{n+1} = \frac{M}{\Delta t}w^n - u \cdot G_x w^n - v \cdot G_y w^n$$
$$- u\frac{\Delta t}{2}\left[uK_{xx} + vK_{xy}\right]w^n - v\frac{\Delta t}{2}\left[uK_{yx} + vK_{yy}\right]w^n$$

   Where ω^n is the vorticity calculated in the previous time step and ω^{n+1} is the vorticity that will be calculated in the time step. It is necessary to apply the boundary condition calculated in the third step before finding vorticity field.

5. **Calculate the stream function with equation:**

$$\left[K_{xx} + K_{yy}\right]\psi = Mw$$

   It is necessary to apply the boundary condition in the equation before finding streamfunction field.

6. **Calculate the velocity with the equation:**

$$Mu = G_y \psi$$
$$Mv = -G_x \psi$$

It is necessary to apply the boundary condition in the equation before u and v. Note that one can solve the linear system using the conjugate gradient method, since M is positive and definite matrix or M can be approximated by its lumped version and therefore easily inverted.

7. **Calculate the concentration with equation:**

$$\left[\frac{M}{\Delta t} + \frac{1}{ReSc}\left[K_{xx} + K_{yy}\right]\right]c^{n+1} = \frac{M}{\Delta t}c^n - u \cdot G_x c^n - v \cdot G_y c^n$$
$$- u\frac{\Delta t}{2}\left[uK_{xx} + vK_{xy}\right]c^n - v\frac{\Delta t}{2}\left[uK_{yx} + vK_{yy}\right]c^n$$

Where c^n is the vorticity calculated in the previous time step and c^{n+1} is the vorticity that will be calculated in the time step. It is necessary to apply the boundary condition in the equation before finding concentration field.

8. **Return the third step and repeat the procedure for next time step.**

The first and second steps are out of time loop, while the third to the seventh step are inside of time loop. The application of the boundary condition in the equation can be before loop, except for the vorticity equation (*fourth step*) that the boundary condition must be applied at each time step.

3. VALIDATION

The validation of the numerical simulation was done by well-known benchmark problem: flow in a lid-driven cavity. The dimensions domain in x-direction and y-direction are [0,1]. We used a mesh with 1563 nodes and 2988 elements and the following Reynolds numbers (*Re*): 10, 100, 400 and 1000. The results were compared with Ghia *et al.* (1982) and Marchi *et al.* (2009).
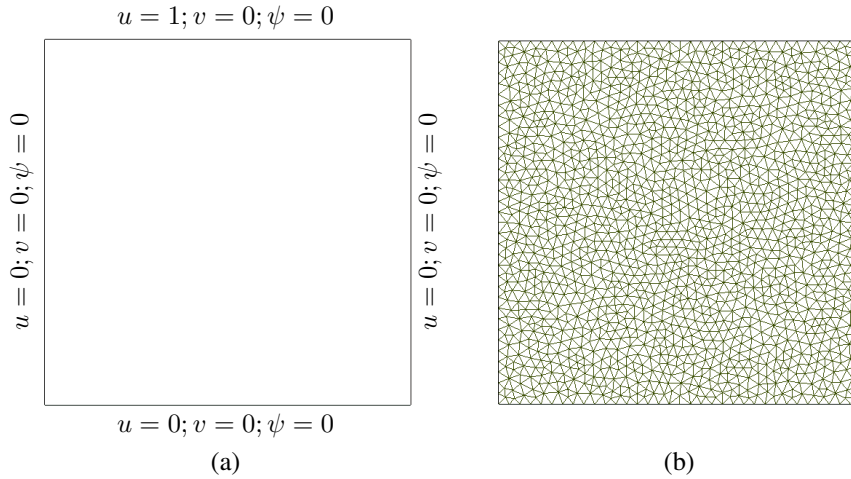

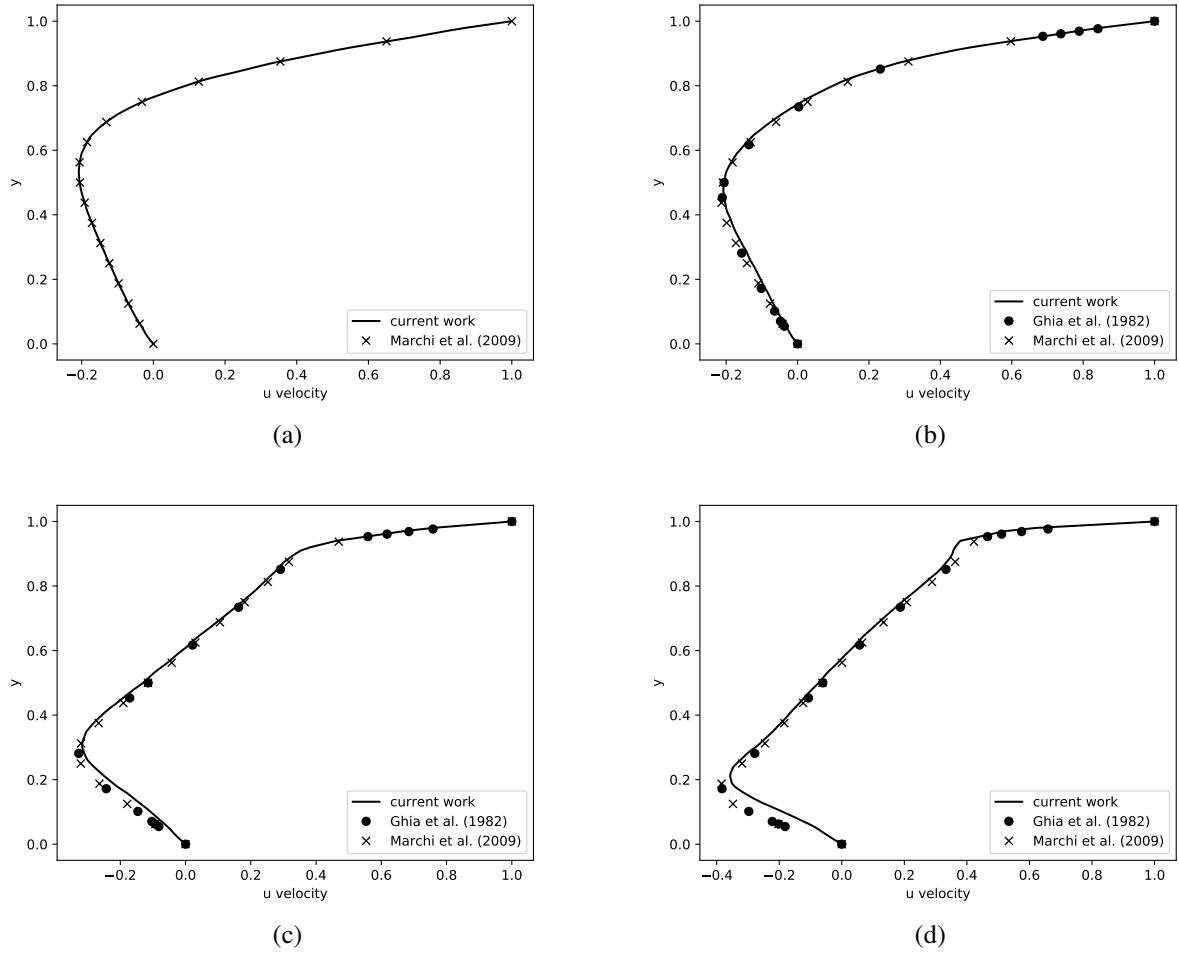Figure 1: Lid-driven cavity: (a) geometry (b) mesh.

(a)

(b)

(c)

(d)

Figure 2: Centerline velocity profile ($x = 0.5$) in a lid-driven cavity for different Reynolds numbers: (a) 10 (b) 100 (d) 400 (f) 1000.
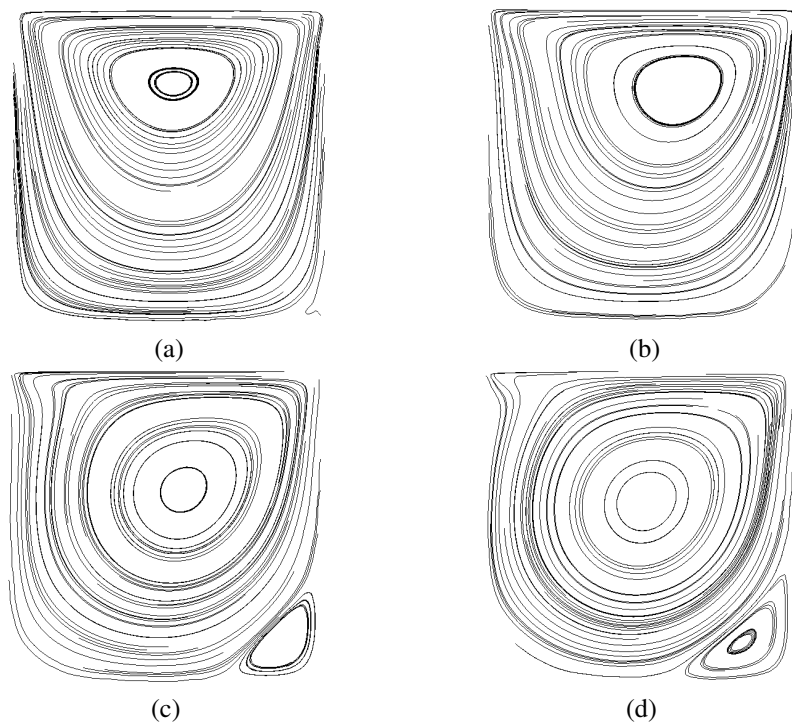

(a)

(b)

(c)

(d)

Figure 3: Streamfunction countours in a lid-driven cavity for different Reynolds numbers: (a) 10 (b) 100 (c) 400 (d) 1000.

4. RESULTS AND DISCUSSION

Some results of simulations are shown to demonstrate its capability of using unstructured triangular meshes on various geometries and combination of geometries. Numerical results are given for several cases of blood flows in artery. The post-processing was performed by open source software *PARAVIEW* proposed by Henderson (2007). The lumen diameter of a typical artery is about $D = 0.003$m, viscosity in the lumen are set to $\mu = 0.0035$Pa.s. and density $\rho = 1060$kg/m^3 as suggested by Bozsak *et al.* (2014). According to Kessler *et al.* (1998), the velocity of the flow at coronary artery is $v = 12$cm/s. Therefore, the Reynolds number is $Re = 109$. Four different geometries were used in the simulations as proposed by Wang *et al.* (2017) and is shown in the Figure 4. Only half domain are shown since the results are symmetric in y-direction.
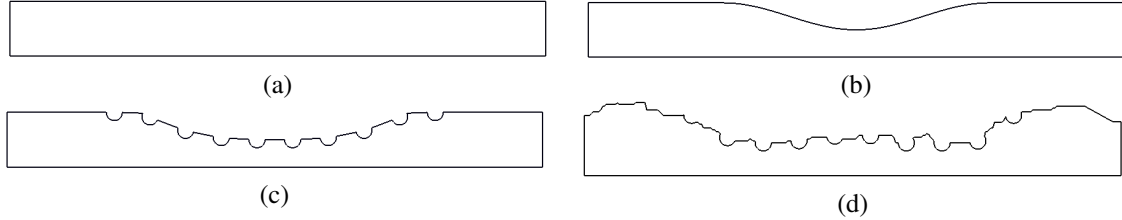
(a)

(b)

(c)

(d)

Figure 4: Non-dimensional geometry for blood flow dynamics in coronary arteries. The channel length L = 10R is based on the channel width R = 1. (a) Straight Channel (b) Curved Channel (c) Curved Channel with Stent and (d) Real Channel with Stent.

4.1 Straight Channel

For the case where we don't have atherosclerosis, the coronary artery is a straight channel. In the literature, this case is known as Hagen-Poiseuille flow and there is an analytical solution for the velocity profile. The analytical solution is given by:

$$u = u_{max}\left(1 - \frac{y^2}{R^2}\right)$$

(10)

where u_{max} is the velocity in the symmetry axis and has the value $u_{max} = 2$, R is non-dimensional radius and has the value $R = 1$ and y the width of half vessel and ranges from $y = [0, 1]$.

The Figure 5 shows the transient velocity profile along the y-direction at the middle of the channel ($x = 5.0R$). As expected, the velocity profile evolution in time converges to the analytical solution with a small error.
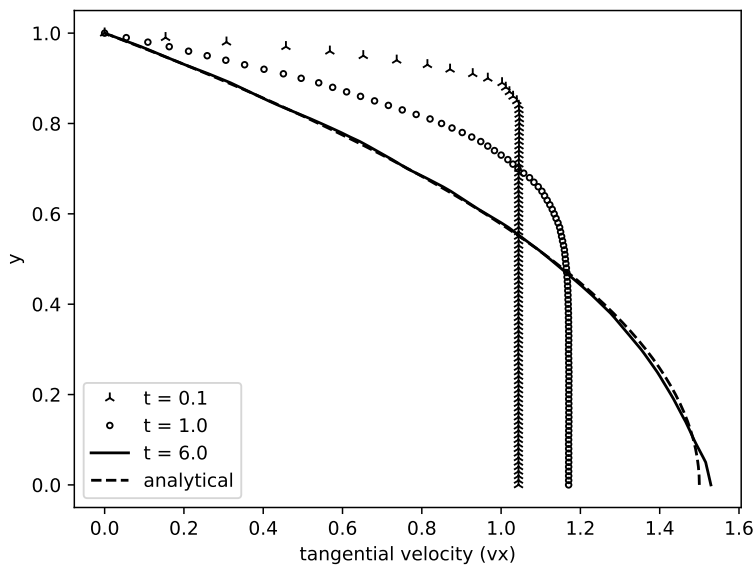
Figure 5: Velocity field profile evolution in time for Straight Channel.

The Figure **??** shows the velocity field evolution in space and time for half domain since the results are symmetric in y-direction. The velocity field is represented with non-dimensional values where the red color is $vx = 2$ and the blue color is $vx = 0$.

t = 0.1   t = 0.5

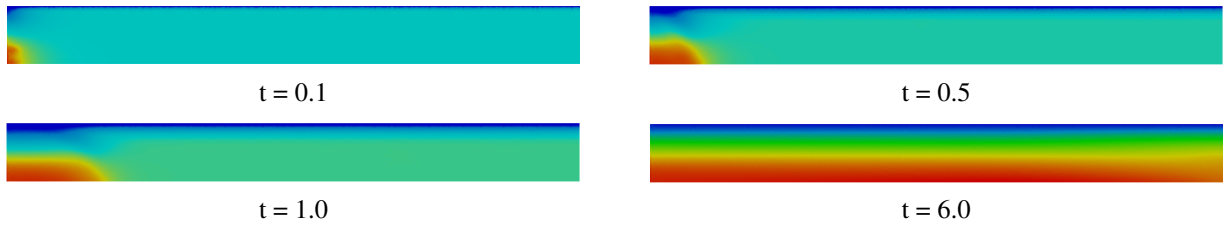t = 1.0   t = 6.0

Figure 6: Time evolution of the velocity field for the straight geometry channel. The velocity profile at the middle of the channel is showed in Fig. 5.

4.2 Curved Channel

For the case where we have atherosclerosis, the coronary artery is a curved channel. This geometry promotes a smooth reduction of the channel diameter followed by a smooth expansion as commonly found in Venturi channel. Was considered 40% of obstruction, that is, the vessel has 60% of diameter for blood flow. The Figure 7 shows the transient velocity profile along the y-direction at the middle of the channel ($x = 5.0R$).
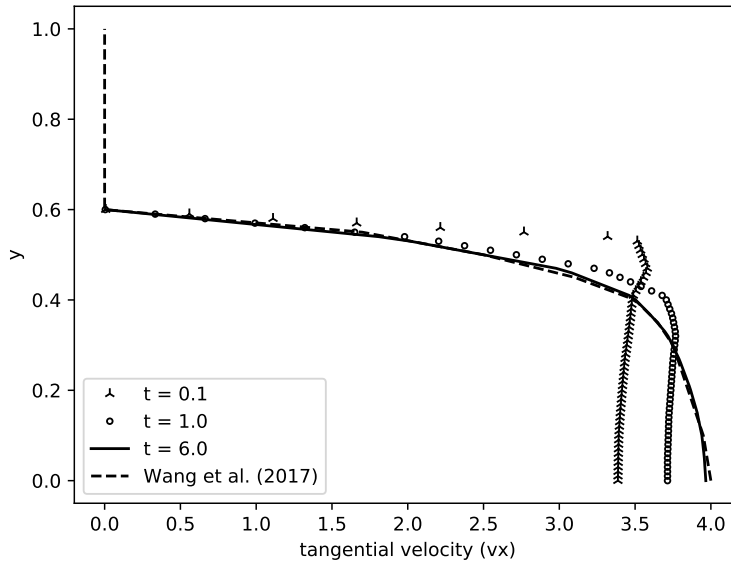

Figure 7: Velocity field profile evolution in time for Curved Channel.

The Figure 8 shows the velocity field evolution in space and time for half domain since the results are symmetric in y-direction. The velocity field is represented with non-dimensional values where the red color is $vx = 4$ and the blue color is $vx = 0$.

t = 0.1   t = 0.5

t = 1.0   t = 6.0

Figure 8: Time evolution of the velocity field for the curved geometry channel. The velocity profile at the middle of the channel is showed in Fig. 7.

4.3 Curved Channel with Stent

In this case, the stent strut was placed at the top of the curved channel and it was modeled by 10 semi-circles uniformely spaced. As in other cases was considered 40% of obstruction, that is, the vessel has 60% of diameter for blood flow. The Figure 9 shows the transient velocity profile along the y-direction at the middle of the channel ($x = 5.0R$).
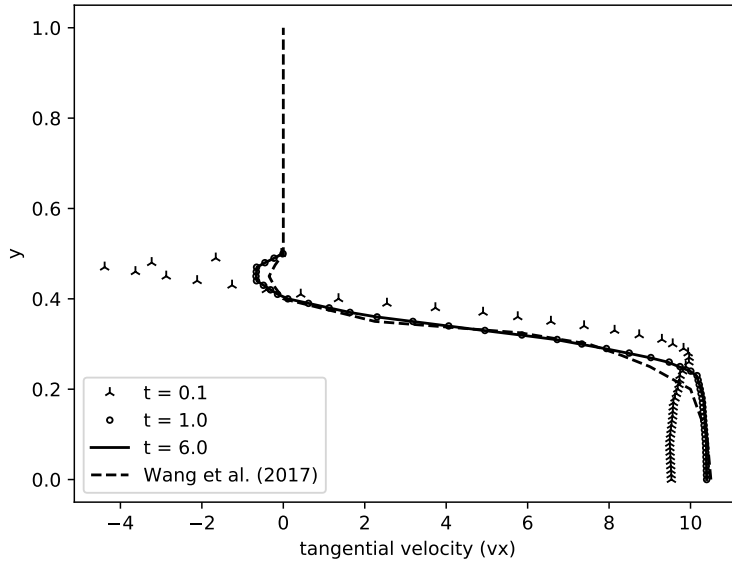
Figure 9: Velocity field profile evolution in time for Curved Channel with Stent.

The Figure 10 shows the velocity field evolution in space and time on the left hand side and the concentration field evolution on the right hand side for half domain since the results are symmetric in y-direction. The velocity field is represented with non-dimensional values where the red color is $vx = 10$ and the blue color is $vx = 0$. The concentration field also is represented with non-dimensional values where the red color is $c = 1$ and the blue color is $c = 0$.
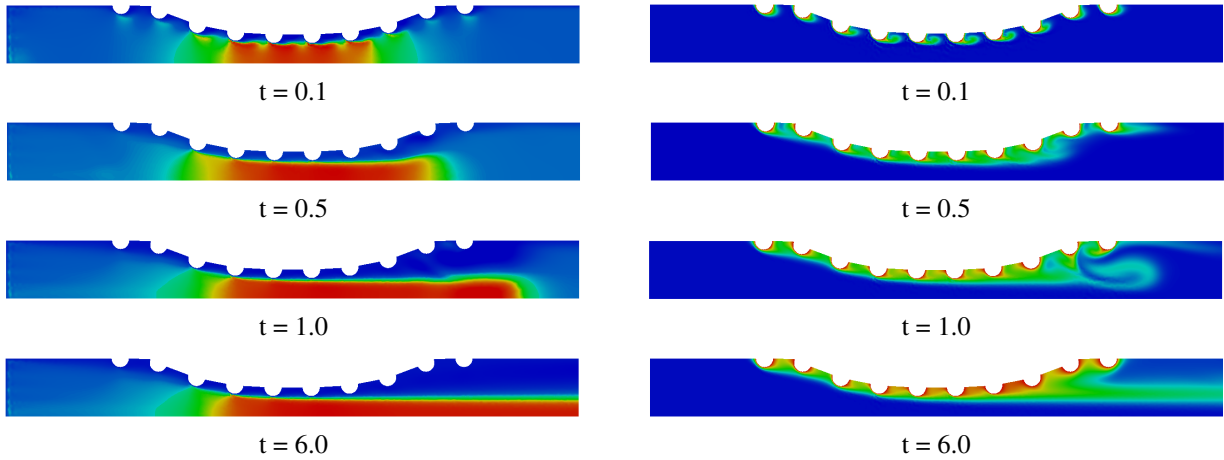

Figure 10: Time evolution of the velocity (left) and concentration (right) fields for the curved geometry channel with stent strut. The velocity profile at the middle of the channel is showed in Fig. 9.

4.4 Real Channel with Stent

In this case, a numerical simulation was performed for a real artery channel whose geometry was taken using image processing from a real coronary artery photography as proposed by Wang *et al.* (2017). It is important to know that each coronary artery geometry is particular to each patient and compatible to its health conditions. The stent strut was placed at the top of the curved channel and it was modeled by 10 semi-circles uniformly spaced. As in other cases was considered 40% of obstruction, that is, the vessel has 60% of diameter for blood flow. The Figure 11 shows the transient velocity profile along the y-direction at the middle of the channel ($x = 5.0R$).
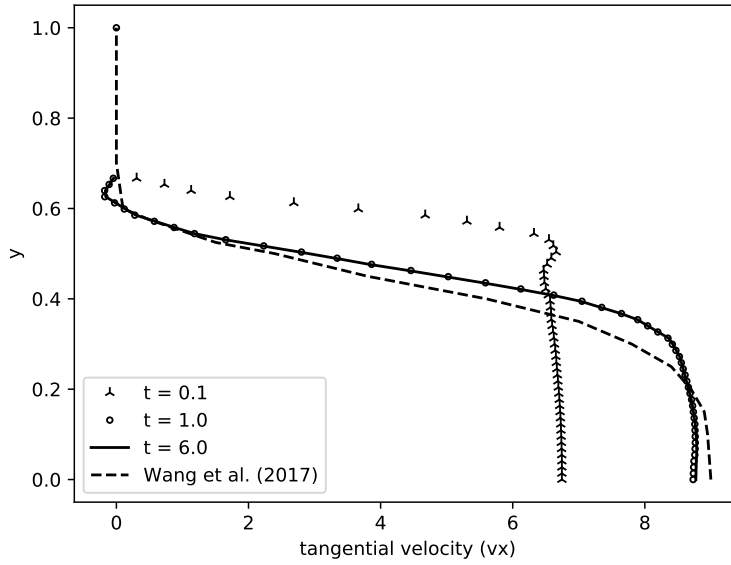
Figure 11: Velocity field profile evolution in time for Real Channel with Stent.

The Figure 12 shows the velocity field evolution in space and time on the left hand side and the concentration field evolution on the right hand side for half domain since the results are symmetric in y-direction. The velocity field is represented with non-dimensional values where the red color is $vx = 9$ and the blue color is $vx = 0$. The concentration field also is represented with non-dimensional values where the red color is $c = 1$ and the blue color is $c = 0$.
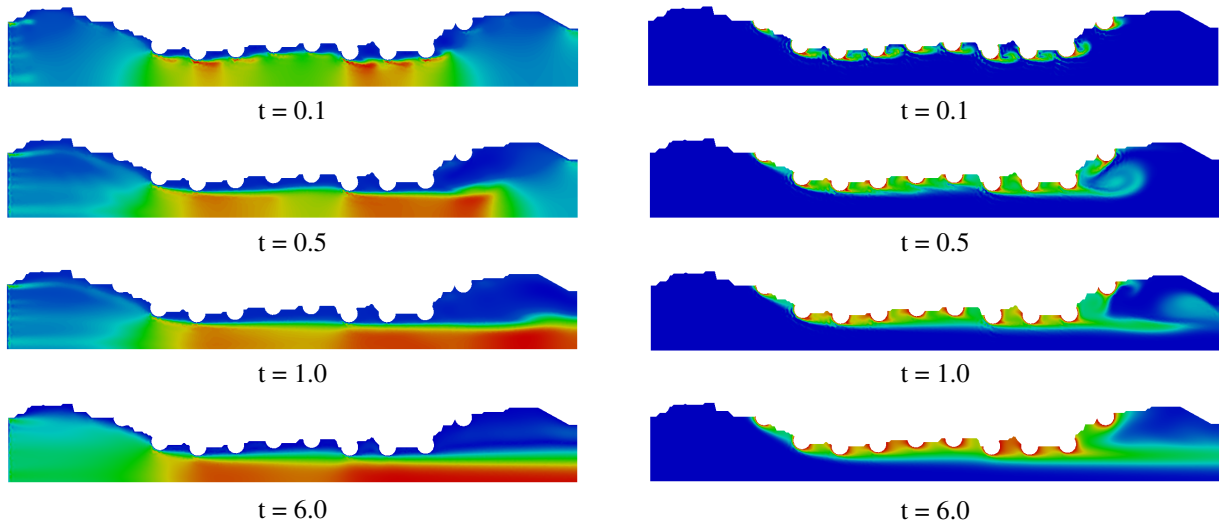

Figure 12: Time evolution of the velocity (left) and concentration (right) fields for the curved geometry channel with stent strut. The velocity profile at the middle of the channel is showed in Fig. 11.

5. CONCLUSION

The results obtained in this paper for the velocity and concentration fields of complex geometries of a modeled coronary artery channel were similar to those presented by Wang *et al.* (2017). However, the numerical simulation was performed using the streamfunction and vorticity formulation by finite element method approach. The Taylor-Galerkin Method was applied to the decrease the spurious oscillations as seen for moderate to high Reynolds numbers. The validation of the numerical solution was done by well-known benchmark lid-driven cavity problem and the results were compared with others authors as well as the Hagen-Poiseuille flow for the case straight channel that was compared with analytical solution. The streamfunction and vorticity formulation showed an useful approximation for to calculate the velocity and concentration fields since the variables are scalars allowing then a smooth implemention.

6. ACKNOWLEDGEMENTS

7. REFERENCES

Anjos, G.R., 2012. *A 3D ALE Finite Element Method for Two-Phase Flows with Phase Change.* Ph.D. thesis, École Polytechnique Fédérale de Lausanne.

Bozsak, F., J-M., C. and Barakat, A., 2014. "Modeling the transport of drugs eluted from stents: physical phenomena driving drug distribution in the arterial wall". *Biomech Model Mechanobiol*, Vol. 13, pp. 327–347. doi:10.1007/s10237-013-0546-4.

Donea, J., 1984. "A taylor-galerkin method for convective transporte problems". *International Journal for Numerical Methods in Engineering.*

Geuzaine, C. and Remacle, J., 2009. "Gmsh: a three-dimensional finite element mesh generator with built-in pre- and post-processing facilities". *International Journal for Numerical Methods in Engineering.*

Ghia, U., Ghia, K.N. and Shin, C.T., 1982. "High-re solutions for incompressible flow using the navier-stokesequations and a multi-grid." *Journal of Computational Physics.*

Henderson, A., 2007. "Paraview guide, a parallel visualization application". *Kitware Inc.*

Jones, E., Oliphant, T. and Peterson, P., 2001. "Scipy - open source scientific tools for python". URL http://www.scipy.org/. [Online; accessed 15/03/2018 09:14].

Kessler, W., Moshage, W., Galland, A., Zink, D., Achenbach, S., Nitz, W., Laub, G. and Bachmann, K., 1998. "Assessment of coronary blood flow in humans using phase difference mr imaging comparison with intracoronary doppler flow measurement." *International Journal of Cardiac Imaging.*

Lohner, R., Morgan, K. and Zienkiewicz, O.C., 1984. "The solution of non-linear hyperbolic equation systems by the finite element method". *International Journal of Numerical Methods in Fluids.*

Marchi, C.H., Suero, R. and Araki, L.K., 2009. "The lid-driven square cavity flow: Numerical solution with a 1024 x 1024 grid." *Journal of the Brazilian Society of Mechanical Sciences and Engineering.*

McGinty, S. and Pontrelli, G., 2016. "On the role of specific drug binding in modelling arterial eluting stents". *Journal of Mathematical Chemistry.*

Python, S.F., 1990. "Python language reference, version 2.7". URL http://www.python.org/. [Online; accessed 12/12/2017 12:18].

Wang, H., McGinty, S., Lucena, R., Pontes, J., Anjos, G. and Mangiavacchi, N., 2017. "Dynamics of blood flow in coronary artery". *International Congress of Mechanical Engineering.*

World Health Organization, W., 2017. "Cardiovascular diseases". URL http://www.who.int/mediacentre/factsheets/fs317/en/. [Online; accessed 28/03/2018 14:37].

Zienkiewicz, O.C. and Taylor, R.L., 2000. "Finite element method - volume 3: Fluid dynamics". *Butterworth-Heinemann.*

8. RESPONSIBILITY NOTICE

The authors are the only responsible for the printed material included in this paper.